Computational Studies of Diindole-Based Molecules for Organic Bulk Heterojunction Solar Devices Using DFT and TD-DFT Calculations

Elly Tan Li Fei
Queen's University Belfast
Joydeep Biswas (joydeep.biswas@smit.smu.edu.in)
Sikkim Manipal Institute of Technology - Majitar https://orcid.org/0000-0002-8055-3187
Bandita Datta
Amity University Kolkata
Dhruva Kumar
Sikkim Manipal Institute of Technology

Research Article

Keywords: Gaussian 09 program, Density functional theory (DFT), Time-dependent density functional theory (TD-DFT), Becke three-parameter Lee-Yang-Parr (B3LYP) functional; Bulk heterojunction (BHJ), Solar device

Posted Date: March 18th, 2021

DOI: https://doi.org/10.21203/rs.3.rs-340673/v1

Version of Record: A version of this preprint was published at Structural Chemistry on April 12th, 2021.
See the published version at https://doi.org/10.1007/s11224-021-01777-z.

Computational Studies of Diindole-Based Molecules for Organic Bulk Heterojunction Solar Devices Using DFT and TD-DFT Calculations

Elly Tan Li Fei[a], Joydeep Biswas*[,b], Bandita Datta*[,c] and Dhruva Kumar[d]

[a] *School of Chemistry and Chemical Engineering, Queen's University Belfast, University Road, Belfast BT7 1NN, United Kingdom.*

[b] *Department of Chemistry, Sikkim Manipal Institute of Technology, Sikkim Manipal University, Majitar, East Sikkim, 737136, India.*

[c] *Department of Chemistry, Amity University - Kolkata Campus, New Town, Kolkata, 700156, India.*

[d] *Department of Mechanical Engineering, Sikkim Manipal Institute of Technology, Sikkim Manipal University, Majitar, East Sikkim, 737136, India.*

* Corresponding authors. E-mail addresses: joydeep.biswas@smit.smu.edu.in (Joydeep Biswas) and bdatta@kol.amity.edu (Bandita Datta)

Keywords: Gaussian 09 program; Density functional theory (DFT); Time-dependent density functional theory (TD-DFT); Becke three-parameter Lee-Yang-Parr (B3LYP) functional; Bulk heterojunction (BHJ); Solar device.

Abstract. Theoretical analysis on geometries, optoelectronic properties, photovoltaic properties and absorption spectra on six π-conjugated molecules used in organic bulk heterojunction solar cell (BHJ), completed using density functional theory (DFT) and time-dependent DFT (TD-DFT) calculations with Becke's three-parameter functional and Lee-Yang-Parr functional (B3LYP), hybrid exchange-correlation functional using the Coulomb-attenuating method (CAM-B3LYP) and WB97XD level with 6-311G basis set supported by Gauss View and Gaussian 09 program. LUMO (lowest unoccupied molecular orbital), HOMO (highest occupied molecular orbital), energy gap (E_{gap}) and V_{oc} (open-circuit voltage) and other essential parameters have been investigated to study the effects on substitution of electron-donating and electron-accepting groups to the proposed molecule. These properties determine if the studied compounds can act as good electron donors along with phenyl-C_{61}-butyric acid methyl ester (PCBM) as a suitable electron acceptor.

1. INTRODUCTION

Solar energy is one of the most compelling resources of power that is sustainable and completely replenishable. It is such crucial renewable energy as it does not produce any greenhouse gases when generating electricity [1]. In recent days, organic photovoltaic cells have become such an exceptional alternative to substitute silicon-based solar devices. BHJ organic solar devices have been one of the essential photovoltaic devices as they are accredited for their more straightforward fabrication process and usage of organic materials, making them biodegradable. BHJ solar cells consist of an active layer prepared of electron donor materials, usually conjugated organic molecules and electron acceptor material, *e.g.*, methylated ester of phenyl-C_{61}-butyric acid (PCBM) or its derivatized products. Conjugated molecules with alternate π-bonds with lower band gaps possess brilliant photovoltaic properties that upgrade BHJ organic solar devices' efficiency. These molecules are suitable for generating large photocurrent upon light absorption [2]. Therefore, knowledge about E_{LUMO}, E_{HOMO} and E_{gap} is needed to complete the analysis about the effects on attachments of electron-releasing and electron-accepting groups to the studied compound.

Fullerene (C_{60}) is an essential allotrope of carbon whose cage-like fused-ring structure comprises alternate C-C and C=C bonds. Fullerene/polymer solar cells have been studied thoroughly and undergo remarkable progress over the years [3a-c]. Fullerene- solar cells can be engineered in ambient conditions using printing methods. These solar cells have the prospective for employing flexible, lightweight, large-scale and inexpensive solar cells [3d,3e]. In recent years, the power conversion efficiency (PCE) of fullerene-based solar cells was reported to be more than 10% [3f-h]. The rapid increase of PCE was achieved by fabrication of new device architectures, manipulation of active and interfacial layers, synthesis of new acceptor and donor

materials, and a deeper understanding of device physics. In the current day and age, organic bulk heterojunction solar cells (BHJ) are one of the essential photovoltaic cells. They are accredited for their more straightforward fabrication process and usage of organic materials, making them biodegradable.

The active layer in organic BHJ solar cell comprises electron-releasing or electron-rich molecules and electron-withdrawing or electron-deficient molecules. The electron-donating molecules are usually conjugated long-chain polymer while electron-accepting molecules are fullerene itself or its derivatives. The production of photocurrent in BHJ solar cells has been illustrated in **Figure 1**. An electron from the conjugated polymer is excited from HOMO to LUMO together with the generation of exciton upon absorption of photons**.** Exciton is diffused through polymer and fullerene interface to split exciton to respective charge carriers, which are hole and electron [4]. The exciton is diffused at the interface because the binding energy of exciton is high, and by doing so allows exciton to populate charge transfer. These free charge carriers will be transferred to respective electrodes. The movement of electrons generates a photocurrent. However, there can be some losses that take place in these processes, such as geminate recombination, where the energy of exciton drops because the exciton does not reach the interface. Moreover, free electrons and holes can recombine and not be transferred to their respective electrodes [5-7].

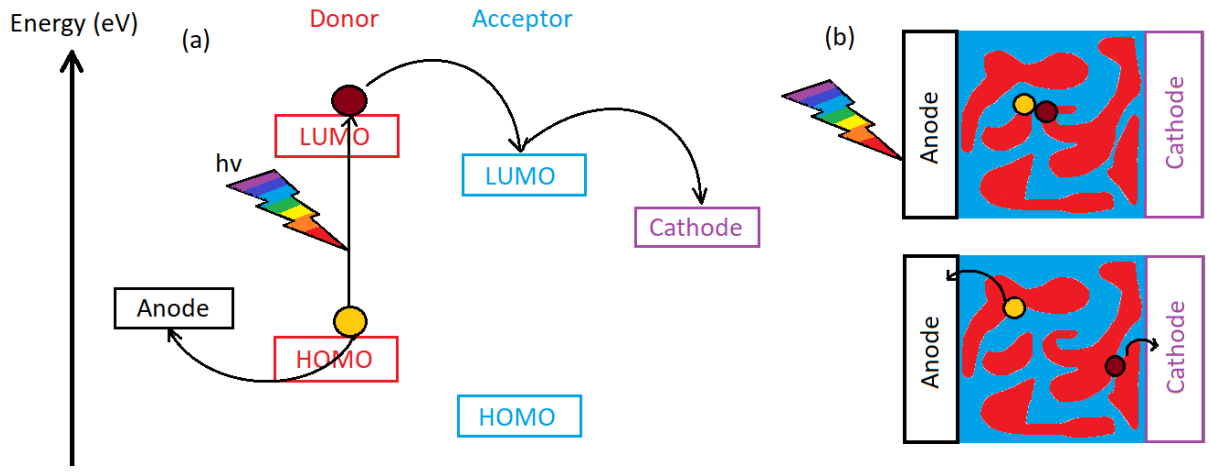

Figure 1: (a) Schematic diagram on photocurrent generation in the active layer of BHJ solar cell. (b) Simpler illumination on the separation of excitons and the transfer of free charge carriers to respective electrodes.

Like our studied molecule in this work, diindole-based molecules are excellent candidates as semiconductors in solar cells because the process of fabrication of these conjugated molecules on flexible substrates is inexpensive [8]. Diindole-based compounds are soluble in common organic solvents allowing them to be cast from solution using wet-processing methods like micro-moulding, inkjet printing and dip coating [9]. These methods are an attractive way of manufacturing photovoltaic cells as the procedures are conducted at ambient pressure and temperature. Furthermore, diindole-based conjugated systems with donor functional groups attached to extend the π-conjugation and are also strong absorber of sunlight. Many studies have shown that organic molecules with extended π-conjugation show strong absorption in the UV-Vis region of the solar spectrum. Thus, the diindole-based molecule is a perfect molecule to study further.

2. Methodology

The present work has been conducted using functional density functional theory (DFT) and time-dependent (TD-DFT) [10] methods and basis sets 6-311G to perform calculations on six introduced compounds. The studied molecules can be synthesized very easily to compounds that are more suitable as part of the active layer in organic BHJ solar cells. Gaussian 09 program was used to carry out various calculations like optimization and energy [11]. DFT using B3YLP functional [12,13] with a 6-311G basis set was used to optimized the six proposed diindole-based molecules to study their geometries, optoelectronic properties and reorganization energies. E_{LUMO}, E_{HOMO} and E_{gap} were also obtained and calculated to examine chemical reactivity indices along with photovoltaic properties. Meanwhile, TD-DFT/6-311G method with different functionals, *viz.*, B3LYP, CAM-B3LYP and WB97XD, were used to investigate the absorption phenomena. The results obtained on the effects of the functional groups attached to the molecules have been studied and discussed. The completed calculations are assumed to be in the gas phase.

3. PROPOSED MOLECULES

Six diindole-based molecules have been introduced in this present work. The molecule is substituted with different electron-donating and electron-accepting groups to improve ground-state geometries, absorption properties and photovoltaic properties. Structures Diln 2, Diln 3, Diln 4, Diln 5 and Diln 6 are the derivatives of the diindole molecule Diln 1, as shown in **Figure 2**. These molecules have been introduced due to their extensive conjugation, which lowers the band gap's energy. Diln 2 and Diln 3 both have electron-withdrawing groups attached, while

Diln 4 and Diln 5 have electron-donating substituents. DiIn 6 has both electron-withdrawing as well as electron-donating groups attached to the ends of the base structure.

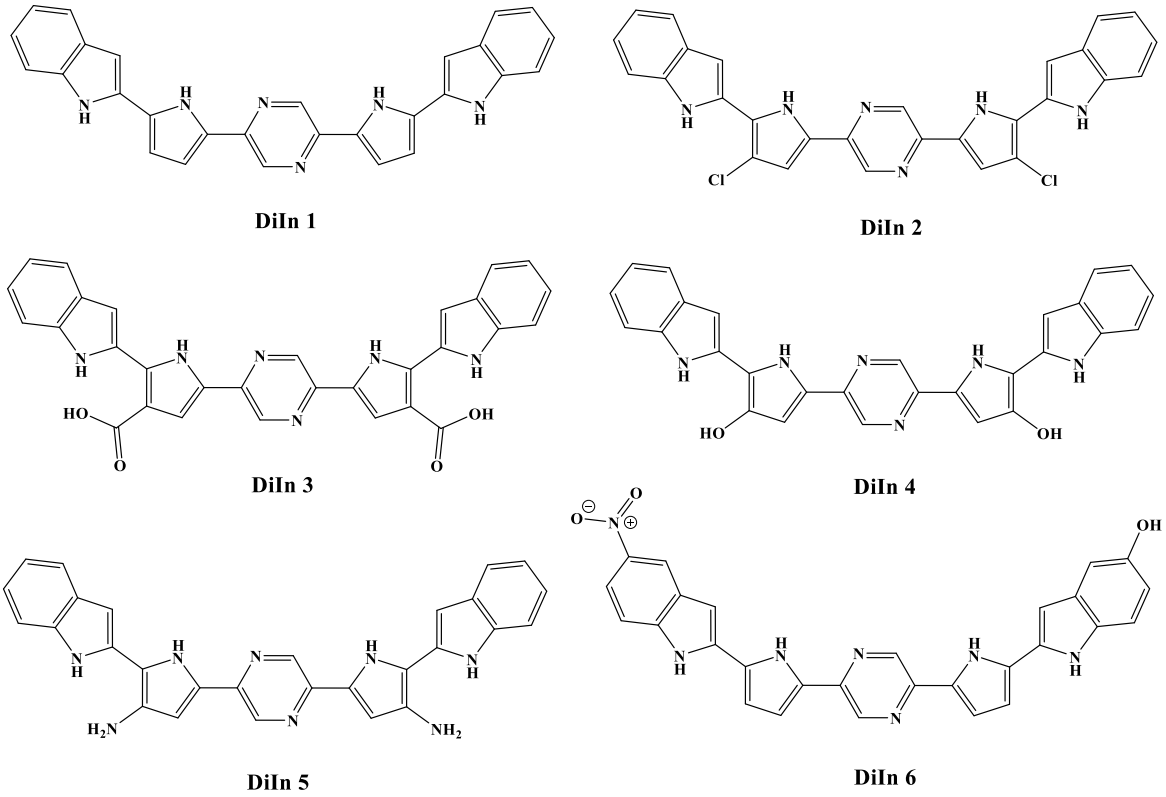

Figure 2: Chemical structures of introduced molecules.

4. RESULTS AND DISCUSSIONS

4.1. Ground State Geometries

The DFT/B3YLP/6-311G method has been used to optimize the six proposed diindole-based molecules' geometries, as demonstrated in **Figure 3**.

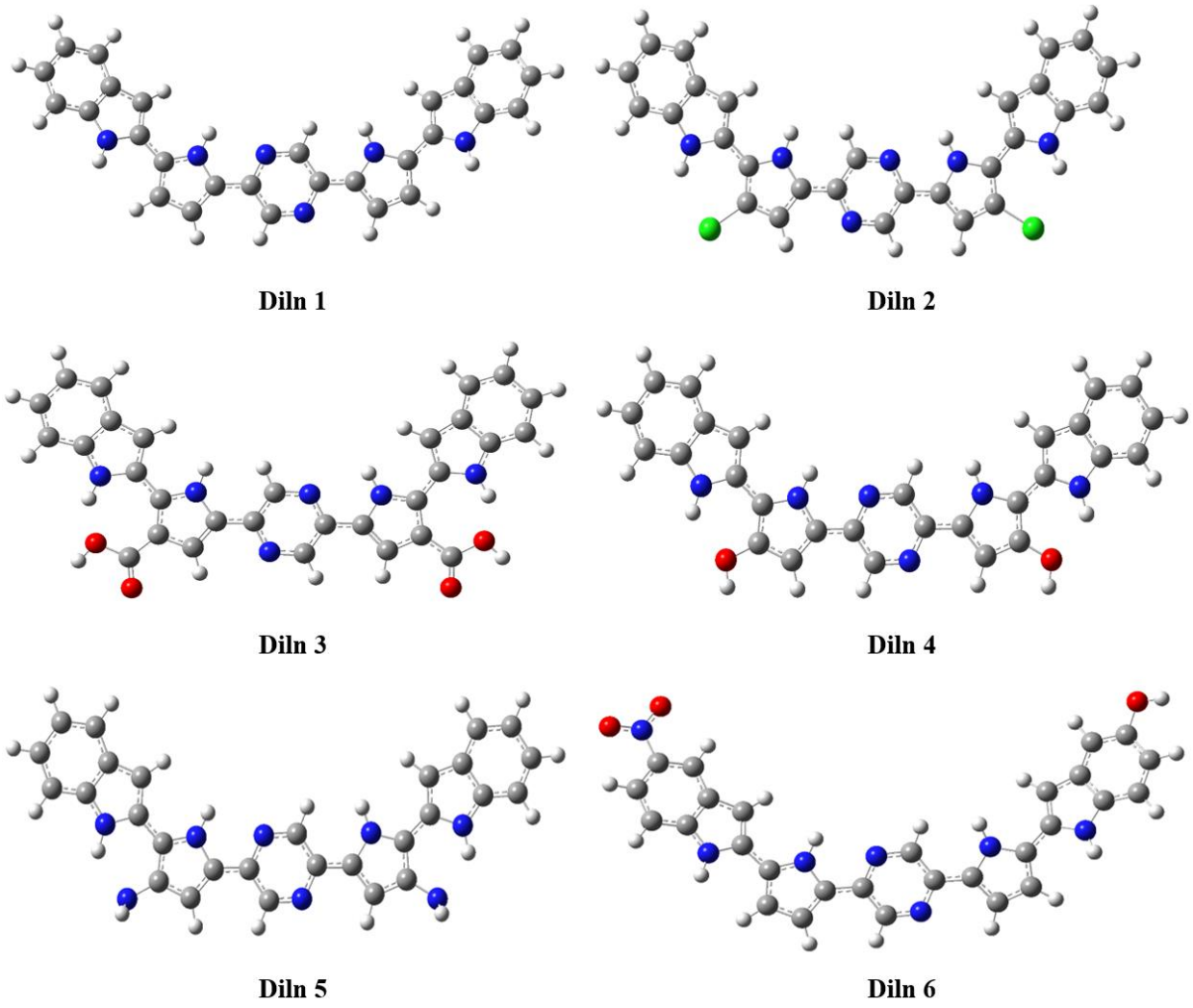

Figure 3: Energy-minimized structures of all the investigated molecules using DFT/B3YLP/6-311G.

The selected geometrical properties such as bond lengths (d_1, d_2, d_3 and d_4) and dihedral angles (θ_1, θ_2, θ_3 and θ_4) are displayed in **Figure 4,** and their values are tabulated in **Table 1**. With ground state geometries data, it analyses the effects on substitution of different donor and acceptor groups.

The proposed molecules with the addition of electron-accepting groups (Diln 2 and Diln 3) have longer bond lengths than those of electron-donating groups (Diln 4 and Diln 5).

Nevertheless, DiIn 6 has both electron-withdrawing and electron-donating groups attached to the base structure's two ends, due to which intra-molecular charge transfer within the molecule occurs. The examined bond lengths of these compounds are found to be in the range of 1.435-1.448 Å, which is close to the bond length of carbon-carbon single bond, *i.e.*, 1.5 Å [14] and shows that the addition of both electron-accepting and electron-donating groups favour intra-molecular charge transfer (ICT) [15] within its molecules.

The dihedral angles of molecules Diln 3, Diln 4 and Diln 5 are close to 180°, which shows that they are nearby planar [16]; meanwhile, the dihedral angles in between the subunits in Diln 1, Diln 2 and Diln 6 are not close to 180°. The dihedral angles between the subunits in Diln 2 have slight torsion due to the attractive interaction between the chlorine atom attached to the pyrrole group and the indole group's nitrogen. The dihedral angles within Diln 1 is not close to planar because the length of the conjugated molecule is long enough for the end indole groups to interact with each other. Moreover, for Diln 6, the hydroxyl group's electron-rich oxygen atom is attracted to the positively charged nitrogen atom from the nitro group.

The intensity of the intramolecular charge transfer is dependent on dihedral angles. It has already been proved that dihedral angle of 180^{o} increases the ICT. As the dihedral angle decreases the ICT also decreases [17]. Hence DiIn 3, DiIn4 and DiIn5 due to a planar dihedral angle will have maximum intra-molecular charge transfer.

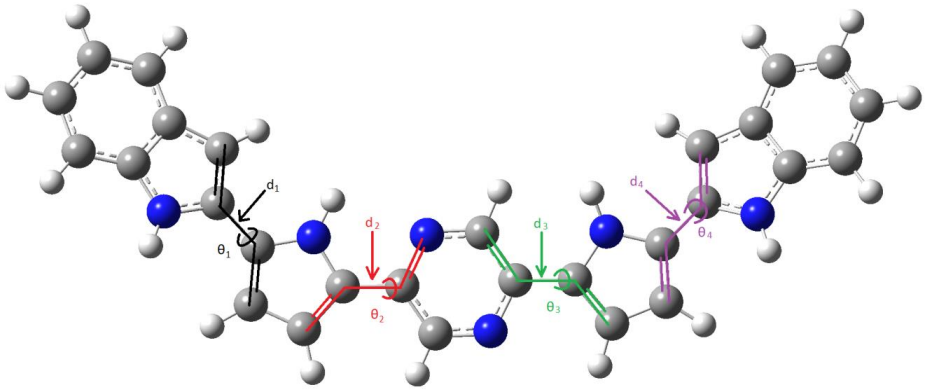

Figure 4: Illustration of selected geometries parameters.

Table 1: The selected geometries properties (d and θ denote bond length and dihedral angles, respectively) of the optimized molecules by DFT/B3YLP/6-311G

	d (Å)				θ (°)			
Molecules	**d_1**	**d_2**	**d_3**	**d_4**	**θ_1**	**θ_2**	**θ_3**	**θ_4**
Diln 1	1.443	1.443	1.446	1.443	157.66	179.03	174.56	155.18
Diln 2	1.442	1.446	1.444	1.441	165.80	176.59	179.89	178.91
Diln 3	1.446	1.448	1.445	1.446	180.00	180.00	180.00	180.00
Diln 4	1.436	1.441	1.443	1.435	180.00	180.00	179.97	179.89
Diln 5	1.440	1.443	1.444	1.440	179.99	180.00	180.00	179.97
Diln 6	1.442	1.445	1.444	1.443	159.29	179.22	175.60	155.68

4.2. Optoelectronic Properties

Parameters like HOMO energy (E_{HOMO}), LUMO energy (E_{LUMO}) and energy gap (E_{gap}) are vital as they are used to determine if actual charge transfer can happen between the acceptor and donor [14,18]. Not only that, but these parameters are also heavily correlated to the performance and photovoltaic properties. Energy gaps of the various molecules have been calculated using the equation 1 below and illustrated in **Figure 5**.

$$E_{gap} = E_{LUMO} - E_{HOMO} \qquad (1)$$

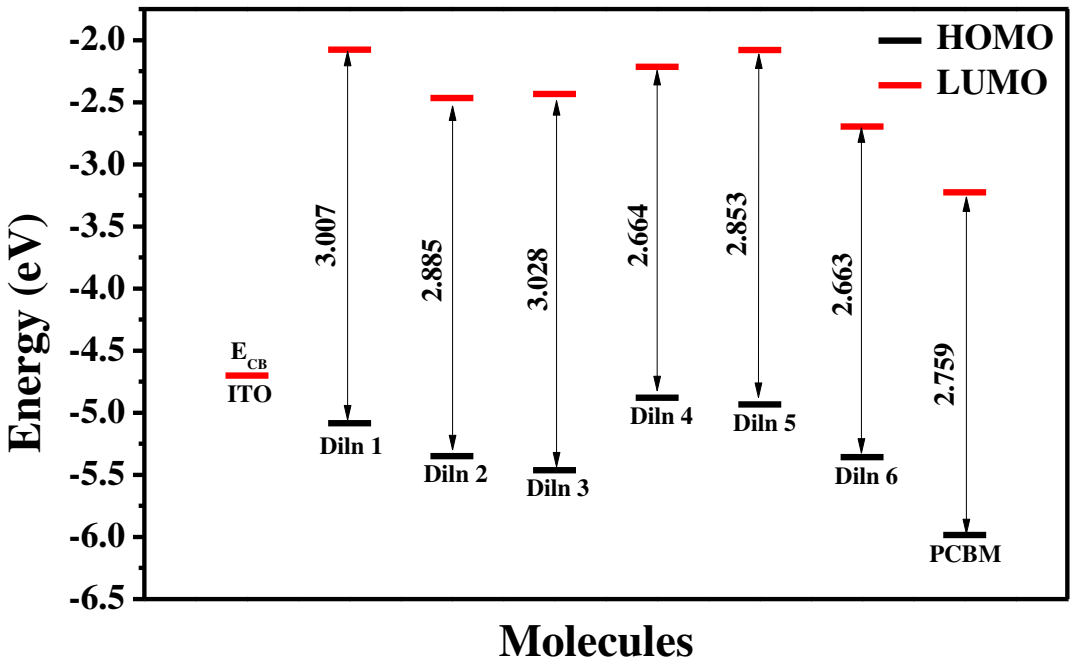

Figure 5: Calculated HOMO and LUMO energy levels (in eV) of all the studied diindole-based molecules, PCBM and ITO.

Calculated E_{LUMO}, E_{HOMO} and E_{gap} of all studied molecules have been tabulated in **Table 2**. Energy gaps of the Diln 2, Diln 3, Diln 4, Diln 5, and Diln 6 are supposed to be lower than Diln 1 due to the addition of electron-accepting groups and electron-donating. With the attachment of those fragments, the conjugation length increases and lowers the bandgap energy [19,20]. The calculated E_{gap} of the studied molecules is in the range of 2.663 to 3.028 eV. The energy gaps of proposed molecules decreases in the order: Diln 3 (3.028 eV) > Diln 1 (3.007 eV) > Diln 2 (2.858 eV) > Diln 5 (2.853 eV) > Diln 4 (2.664 eV) > Diln 6 (2.663 eV). From the results, E_{gap} of proposed molecules with an electron-accepting group (Diln 2 and Diln 3) is higher than molecules with an electron-donating group (Diln 4, Diln 5 and Diln 6), which is due to the compounds that have electron-donating groups attached (Diln 4, Diln 5 and Diln 6) demonstrate destabilization of HOMO and LUMO energy levels. In contrast, molecules with an electron-accepting group attached show stabilization of HOMO and LUMO energy levels. Theoretically,

E_{gap} Diln 2 to Diln 6 are supposed to be lower than Diln 1 due to the addition of fragments that increase the chain's length. However, Diln 3 shows otherwise due to intra-molecular charge transfer within the molecule. E_{gap} of Diln 4 and Diln 6 are the lowest; this shows a notable effect of intra-molecular charge transfer that would make the absorption spectra shift towards the red region [21]. Moreover, E_{LUMO} all the studied compounds, including PCBM, are higher than the E_{CB} of ITO (-4.7 eV) [13], which allows the movement of an electron to flow smoothly and generate current.

Furthermore, the LUMO energy difference between acceptor and donor (ΔE_{LUMO}) is also a meaningful way to check if electrons' flow will be possible from donor to acceptor. Based on **Table 2**, ΔE_{LUMO} for molecules, Diln 1 to Diln 6 is more than 0.3, suggests that photochemically excited electron jumps quickly from DiIn 1-6 acting as donors to PCBM, which acts as an acceptor [14]. The equation 2 stated below is used to calculate ΔE_{LUMO}.

$$\Delta E_{LUMO} = E_{LUMO} \text{ (studied molecule)} - E_{LUMO} \text{ (PCBM)} \qquad (2)$$

Table 2: Calculated theoretical optoelectronic parameters of introduced molecules using DFT/B3YLP/6-311G

Molecules	**$-E_{LUMO}$ (eV)**	**$-E_{HOMO}$ (eV)**	**E_{gap} (eV)**	**ΔE_{LUMO} (eV)**
Diln 1	2.078	5.085	3.007	1.148
Diln 2	2.465	5.350	2.885	0.761
Diln 3	2.434	5.462	3.028	0.792
Diln 4	2.215	4.879	2.664	1.011
Diln 5	2.080	4.933	2.853	1.146
Diln 6	2.694	5.357	2.663	0.532
PCBM	3.226	5.985	2.759	---

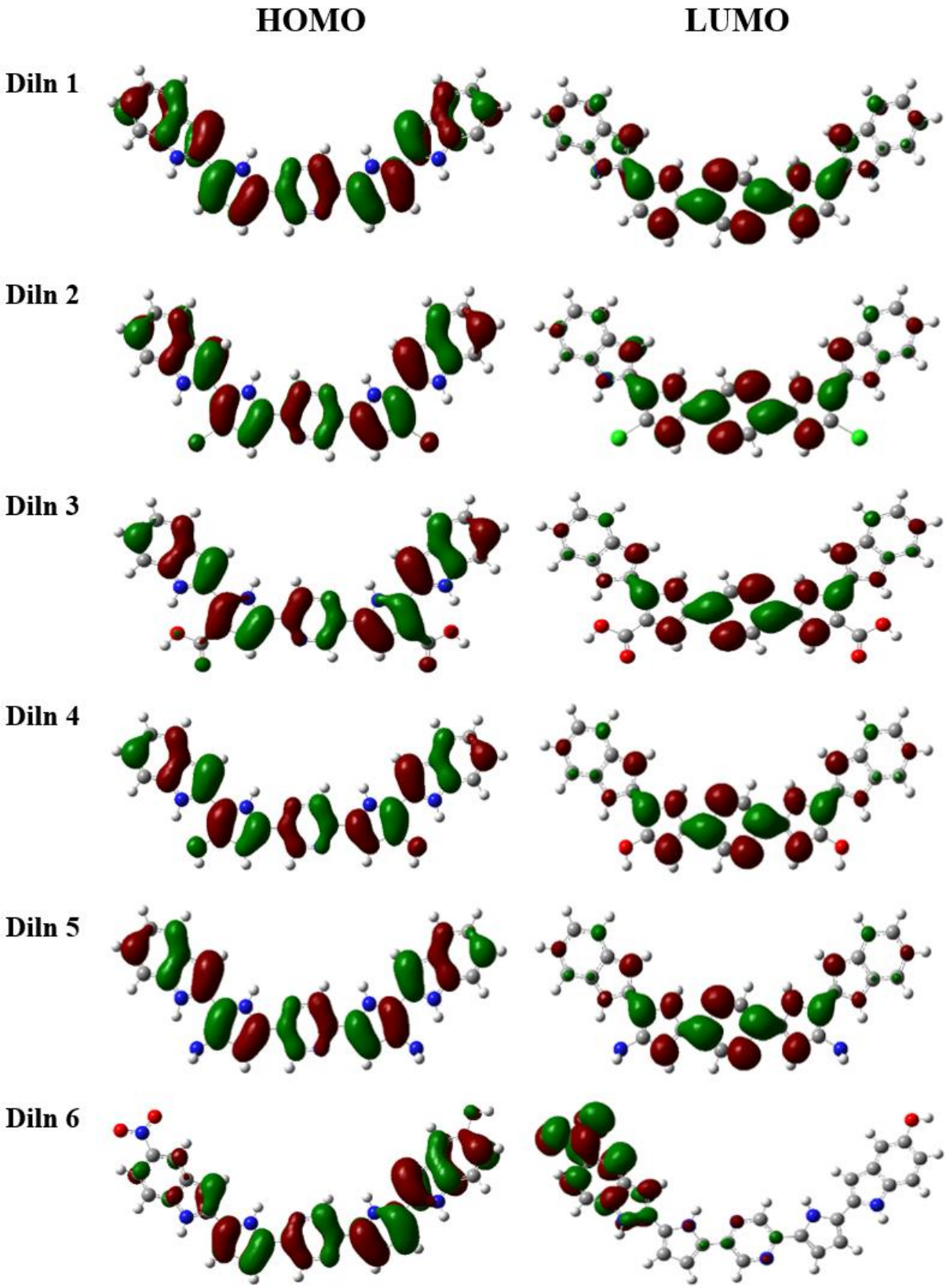

Figure 6: The contour plots of HOMO and LUMO orbitals of studied diindole molecules.

Other than that, the contour of HOMO and LUMO molecular orbitals can provide the ability to transfer holes and electrons, respectively [13]. The electron density contour of HOMO and LUMO orbitals also helps identify the molecules' excitation properties. According to the electron density contour by DFT/B3YLP/6-311G illustrated in **Figure 6,** HOMO shows an evident uniform electron density distribution throughout all the molecules. The contour plots of HOMO and LUMO exhibits the delocalization of the conjugated systems of the molecules. HOMO and LUMO show π-bonding character and π-antibonding character in the subunit, respectively. [22,23].

However, notice that the contour plot of the last molecule, Diln 6, is isolated, extending to the pi-conjugation. Upon analyzing the frontier molecular orbitals of DiIn6, it was observed that the HOMO was mainly localized on the donor group (hydroxyl-substituted indole). In contrast, the LUMO was mainly localized on the nitro substituted indole in this molecule. These electron density distributions account for efficient charge separation and electron injection. Moreover, electronic transitions from HOMO to LUMO correspond to intra-molecular charge transfer. On the other hand, the LUMO of this molecule DiIn6 is higher than PCBM's LUMO, indicating a good electron injection from DiIn6 to PCBM. Hence, it is one of the best candidates for photovoltaic devices compared to other diindole-based compounds.

4.3. Analysis of Chemical Potential, Electronegativity and Chemical Hardness

With the obtained and calculated values of E_{LUMO}, E_{HOMO} and E_{gap}, they are used to investigate further chemical reactivity indices such as chemical potential (μ), electronegativity (χ) and chemical hardness (η) [24]. They are essential parameters that evaluate if the flow of electron is

possible from donor to acceptor PCBM. Equations to calculate chemical potential, electronegativity and chemical darkness are stated as below [21,25]:

$$\mu = \frac{(E_{HOMO} + E_{LUMO})}{2} \qquad (3)$$

$$\eta = \frac{(E_{HOMO} - E_{LUMO})}{2} \qquad (4)$$

$$\chi = \frac{-(E_{HOMO} + E_{LUMO})}{2} \qquad (5)$$

The calculated results using the Gaussian 09 program have been recorded in **Table 3** [11]**.** Chemical potentials, μ of all the investigated diindole-based molecules, are higher than that of the acceptor molecule (PCBM), which shows that the electrons can flow smoothly from studied molecules to PCBM. On the other hand, electronegativity, χ of all the proposed molecules, is smaller than PCBM. It shows that electrons are attracted from the investigated diindole-based molecules to PCBM in BHJ organic solar device. However, chemical hardness, η of PCBM is lower than Diln 1, Diln 2, Diln 3 and Diln 5, due to the inter charge transfer between the proposed molecules and PCBM.

Table 3: Calculated chemical potential (μ), chemical hardness (η) and electronegativity (χ) of all studied compounds and PCBM were obtained using DFT/B3YLP/6-311G

Molecules	Chemical Potential, μ	Chemical Hardness, η	Electronegativity, χ
Diln 1	-3.582	1.503	3.582
Diln 2	-3.907	1.442	3.907
Diln 3	-3.948	1.514	3.948
Diln 4	-3.547	1.332	3.547
Diln 5	-3.507	1.427	3.507
Diln 6	-4.026	1.331	4.026
PCBM	-4.606	1.380	4.606

4.4. Analysis of Molecular Electrostatic Potential

Knowledge about electron density is crucial for the study of electrostatic potential. DFT/B3YLP/6-311G calculated molecular electrostatic potential (MEP) to determine the proposed molecules' electrostatic effect. MEP is a plot of 'electrostatic potential' mapped into the constant 'electron density surface', predicting the nucleophilic and electrophilic reactive sites and electrostatic potential [26-29]. The charge-transfer (CT) excitons are dependent on the donor and acceptor molecules' interaction in the excited states. This interaction is due to the electron-rich groups of donors with the electron-deficient groups of acceptors. The colour code of the map of all studied compounds are mentioned below:

- Diln 1 = Between -6.535 e^{-2} (deepest red) and 6.535 e^{-2} (deepest blue)
- Diln 2 = Between -7.715 e^{-2} (deepest red) and 7.715 e^{-2} (deepest blue)
- Diln 3 = Between -7.797 e^{-2} (deepest red) and 7.797 e^{-2} (deepest blue)
- Diln 4 = Between -7.901 e^{-2} (deepest red) and 7.901 e^{-2} (deepest blue)
- Diln 5 = Between -6.668 e^{-2} (deepest red) and 6.668 e^{-2} (deepest blue)
- Diln 6 = Between -7.359 e^{-2} (deepest red) and 7.359 e^{-2} (deepest blue)

Different electrostatic potential values appear in different colours, where the red colour region denotes electron-rich or negative electrostatic potential. In contrast, the blue region shows the electron-deficient region or positive electrostatic potential. The blue region is usually an electrophilic attack site, while the red region is a site for the nucleophilic attack [30]. The colour code of the map for all the introduced molecules is recorded in **Figure 7** with the contour molecules.

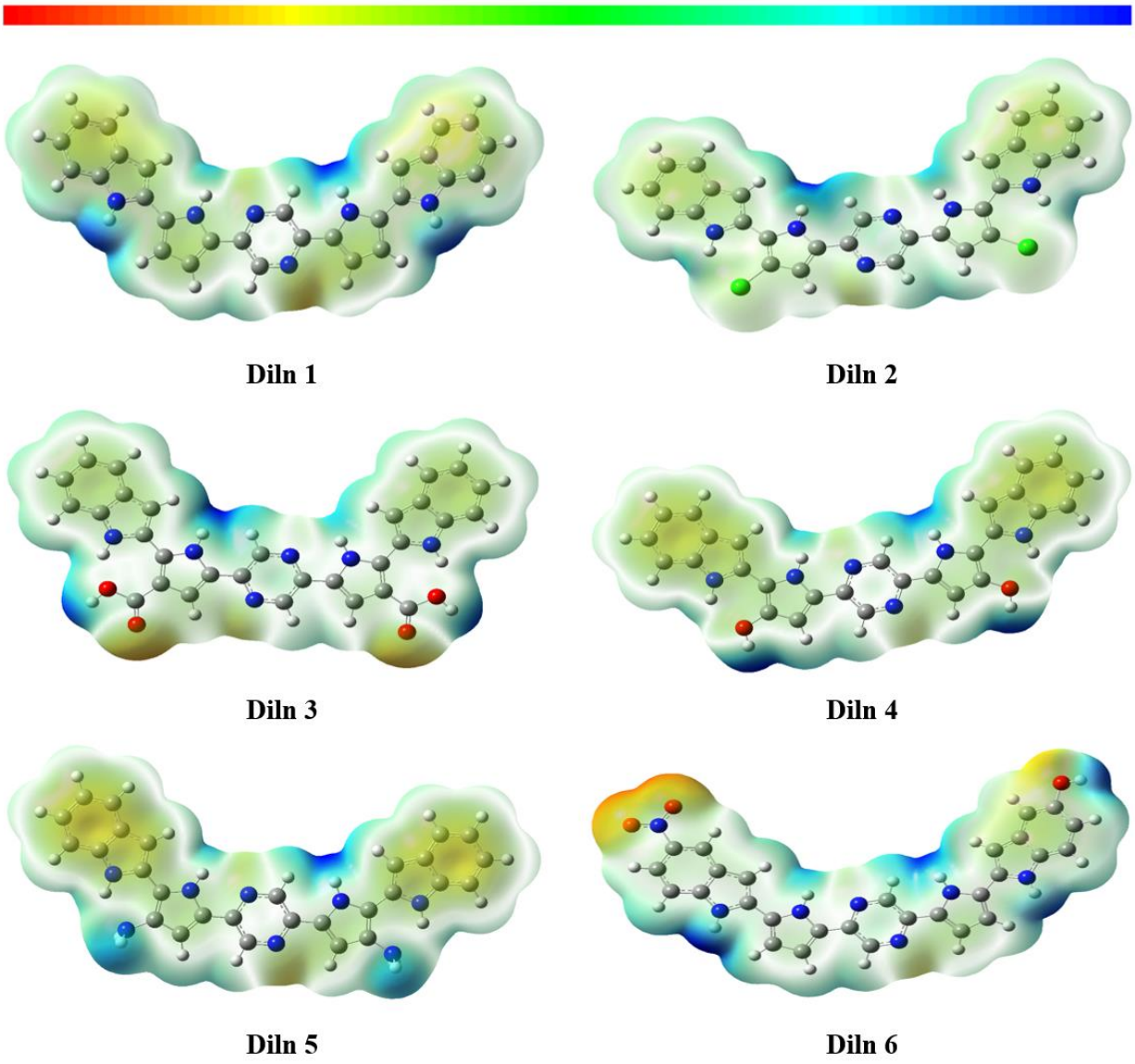

Figure 7: Molecular electrostatic potential of studied molecules using DFT/B3YLP/6-311G.

4.5. Performance/Photovoltaic Properties

For examining the performance and efficiency of organic photovoltaic devices, four essential parameters help to evaluate, *i.e.*, short circuit current density (J_{sc}), open-circuit voltage (V_{oc}), fill factor (*FF*) and power conversion efficiency (η). These studied molecule parameters determine the probability of electron transfer from introduced molecules to the conductive band of the

acceptor PCBM [5,14,21]. The data on these parameters can be found in **Table 4** using the method DFT/B3YLP/6-311G.

4.5.1. Short Circuit Current Density

Short circuit current density (J_{sc}) is maximum photocurrent density produced at zero open-circuit voltage (V_{oc} = 0) [31]. It indicates the number of charge carriers generated and collected at the electrodes, respectively. J_{sc} is heavily dependent on morphology, mobility and lifetime of charge carriers. The equation to calculate short circuit current density is stated below where $LHE(\lambda)$ represents the light-harvesting efficiency at a specific wavelength, Φ_{inj} is electron injection efficiency and finally, η_{collect} is charge collection efficiency [32].

Light-harvesting efficiency (*LHE*) is also an essential property that enhances BHJ solar cells' performance. The values of *LHE* should be high to obtain maximum photocurrent [33,34]. The calculated *LHE* is included in **Table 4** using equation 7, where *f* represents the oscillator strength corresponding to the maximum absorption of wavelength. The calculated values of *LHE* of these compounds are in a range of 0.9137-0.9512. The data collected decreases in the following order Diln 4 (0.9512) > Diln 1 (0.9484) > Diln 5 (0.9467) > Diln 2 (0.9419) > Diln 6 (0.9418) > Diln 3 (0.9137), which indicates that the substitution with a strong electron-donating group is an efficient way to improve the photocurrent response.

$$J_{sc} = \int LHE(\lambda)\Phi_{inj}\eta_{coll}d\lambda \qquad (6)$$

$$LHE = 1 - 10^{-f} \qquad (7)$$

4.5.2. Open Circuit Voltage

Open circuit voltage (V_{oc}) is one of the most significant properties determining a BHJ solar cell's productivity. The maximum circuit voltage is obtained when the short circuit current density is zero ($J_{sc} = 0$) [35]. V_{oc} determines if the electron injection process is possible to take place from excited molecules to PCBM. A high LUMO energy of acceptor and low LUMO energy of π-conjugated compounds usually enhance V_{oc} [36], which provides high performance of solar cells. V_{oc} can be calculated in the following equation 8 where E_{HOMO} (donor) is the HOMO energy of the studied molecules, E_{LUMO} (acceptor) is the LUMO energy of PCBM and 0.3 represents typical loss found in BHJ organic solar device [21,37].

$$V_{oc} = (|E_{HOMO}\text{ (donor)}| - |E_{LUMO}\text{ (acceptor)}| - 0.3) \qquad (8)$$

4.5.3. Fill Factor

Fill factor (*FF*) is another very vital feature that evaluates the effectiveness of organic solar devices. It depends on the charge carrier mobility of the hole (acceptor) and electron (donor) transport materials. Moreover, it relies on the product of mobility and lifetime of bulk material, the morphology of the cathode/polymer cathode, and the active-polymer layer's thickness. The parameter V_{mpp} represents the voltage at maximum output power and I_{mpp} is current density at maximum output power is needed to complete the fill factor calculation (equation 9) [5].

$$FF = \frac{V_{mpp} \times I_{mpp}}{V_{oc} \times J_{sc}} \qquad (9)$$

4.5.4. Power Conversion Efficiency

Power conversion efficiency (η) is also a vital performance parameter that plays a significant role in evaluating and optimizing photovoltaic devices' effectiveness. Every single factor that

affects the device's efficiency can be increased by upgrading BHJ material, every layer, electrodes and interface to attain the best performance. The power conversion efficiency of a BHJ photovoltaic device is expressed in the equation 10 mentioned below, where *FF* is fill factor, V_{oc} is open-circuit voltage, J_{sc} represents short-circuit current and P_{in} indicates the incident power intensity of the sun [5,14,21].

$$\eta = \frac{P_{out}}{P_{in}} = \frac{FF\ (V_{oc} \times J_{sc}\ )}{P_{in}} \qquad (10)$$

Table 4: Calculated performance parameters have been performed and obtained using DFT/B3YLP/6-311G

Molecules	V_{oc} (eV)	*f*	*LHE*
Diln 1	1.559	1.2875	0.9484
Diln 2	1.824	1.2359	0.9419
Diln 3	1.936	1.0640	0.9137
Diln 4	1.353	1.3114	0.9512
Diln 5	1.407	1.2731	0.9467
Diln 6	1.831	1.2350	0.9418

4.6. Density of States (DOS)

The analysis of states' density is used to evaluate charge transport properties and this property has been completed using GaussSum software [38]. Knowledge of density of states can be used to investigate and discuss the bequest of α and β electrons to valence and conduction band, respectively. However, DOS is only valid provided the electrons are free [14]. The DOS of all studied molecules has been demonstrated in **Figure 8.** The DOS analysis corroborates well with the FMO results for the DiIn compounds. It is found to be close to zero mark for a symmetric bandgap. This means that the main body of the DOS helps in determining the stability of the effect of the energetic disorder on electron and hole transport.

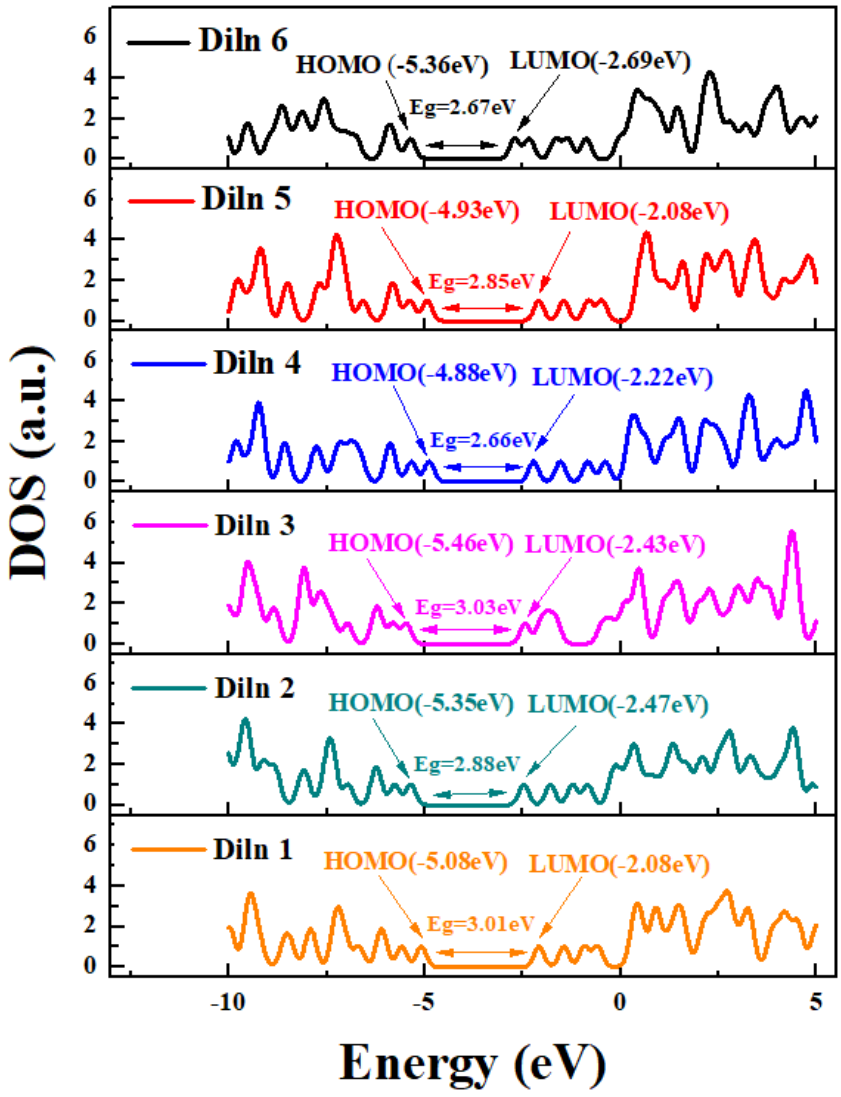

Figure 8: DOS (density of states) studies carried out using GaussSum software.

4.7. Reorganization Energies of Diindole-Based Molecules

To estimate approximately the charge transfer characteristic of organic materials, the reorganization energies were calculated and analyzed. The lesser reorganization energy affirms the more rapid electron transport [39]. Hole reorganization energy (λ_h) and electron reorganization energy (λ_e) can be calculated using equations 11 and 12 [40]. The reorganization energies were calculated using DFT/B3YLP/6-311G level of theory.

$$\lambda_h = (E_0^+ - E_+) + (E_+^0 - E_0) \qquad (11)$$

$$\lambda_e = (E_0^- - E_-) + (E_-^0 - E_0) \qquad (12)$$

where E_0^+ is energy of cation calculated with neutral optimized structure, E_0^- is energy of anion calculated with neutral optimized structure, E_+ is energy of cation calculated with cation optimized structure, E_- is energy of anion calculated with anion optimized structure; E_+^0 is energy of neutral molecule calculated with cation optimized structure, E_-^0 is energy of neutral molecule calculated with anion optimized structure and E_0 is energy of neutral molecule at ground state.

The reorganization energies (λ_h and λ_e) of the investigated diindole-based molecules are shown in Table S1 (supplementary data). It is observed that the calculated reorganization energies was found to be lowest for Diln 4 and highest for Diln 6. Hence, electron transport will be more rapid for Diln 4 compared to other investigated diindole-based molecules.

4.8. Absorption Spectra

With the TD-DFT/6-311G method using different functionals, *viz.*, B3LYP, CAM-B3LYP and WB97XD, all optimized proposed molecules have been used to further calculated to obtain the UV-Vis spectra illustrated in **Figure 9**. The above-mentioned level of theories provide information about excitation energy (E_{ex}), maximum wavelength (λ_{max}), oscillator strength (f) and electronic transitions, which are stated in **Table 5**, **S2** (supplementary data) and **S3** (supplementary data). The λ_{max} of all the studied molecules is within the visible light region from 350 to 780 nm. All electronic transitions for the molecules are also π-π* [21].

From the results obtained, the maximum absorption wavelengths (λ_{abs}) of the six investigated molecules in descending order is the same using different functionals, *viz.*, B3LYP, CAM-B3LYP and WB97XD, which starts from Diln 4 > Diln 5 > Diln 2 > Diln 3 > Diln 1 > Diln 6 (for HOMO to LUMO transition, **Table 5**, **S2** and **S3**). Among all the diindole-based molecules, Diln 4 has the longest λ_{max} in all the used level of theories. As mentioned above, the order indicates that Diln 4 shows donor-acceptor ICT interaction, which is the strongest, compared to other molecules. The absorption spectra show that the acceptor in the π-conjugated system is favourable for a long-wavelength light harvesting, which decides solar cells' efficiency through the photo-electrical conversion. Electron donating groups attached (Diln 4 and Diln 5) molecules have longer wavelengths than electron-accepting groups (Diln 2 and Diln 3). Diln 6 is an exception as it has both electron-withdrawing and electron-donating groups attached to the base structure. However, it has the shortest wavelength due to the attraction between electron-rich oxygen atom from a hydroxyl group and positively charged nitrogen atom from the nitro group. The oscillator strength is related to the probability of transformation from the ground state to an excited state. The larger the oscillator strength, the higher the maximum wavelength shown by Diln 4. The maximum wavelength is also heavily dependent on excitation energies. Higher excitation energy will lead to a shorter maximum wavelength.

Chrostowska *et al.* reported that the calculations using CAM-B3LYP functional is the pre-eminent for indole related molecules [41]. This is because the theoretical data obtained by CAM-B3LYP is the closest to the experimental results of the indole molecules. Thus, the TD-DFT/CAM-B3YLP/6-311G method is also used to conduct the absorption spectroscopic studies of the investigated diindole-based molecules. Moreover, it is noticed that the maximum absorption wavelength (λ_{abs}) of Diln 4 was found to be the highest compared to other molecules

using the TD-DFT/CAM-B3YLP/6-311G method. Among all the diindole-based molecules, Diln 5 has the highest oscillator strength (1.7719) using the TD-DFT/WB97XD6-311G method. Comparing all the methods, it is observed that the λ_{abs} of Diln 4 was found to be the highest (522.01 nm) using the TD-DFT/B3YLP/6-311G method. We observed that E_{gap} values of all the diindole-based molecules were found to be higher in the case of the TD-DFT/WB97XD/6-311G method, while the same values were found to be lower in the case of the TD-DFT/B3YLP/6-311G method. Hence, B3YLP functional was used to study the optoelectronic properties.

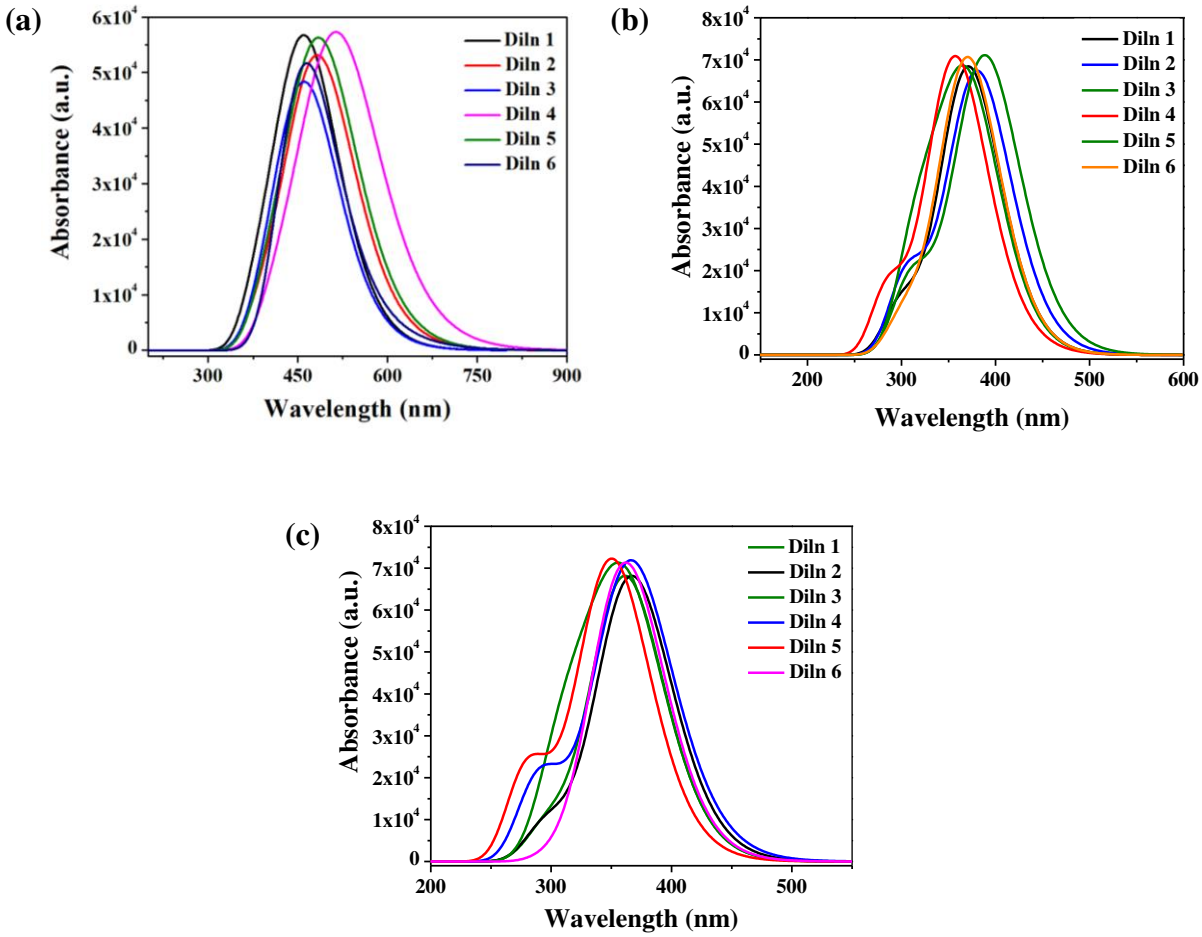

Figure 9: Theoretically obtained UV-Vis spectra of all the investigated diindole-based molecules using (a) TD-DFT/B3YLP/6-311G, (b) TD-DFT/CAM-B3YLP/6-311G and (c) TD-DFT/WB97XD/6-311G.

Table 5: Theoretical values of excitation energy (E_{ex}), absorption wavelength (λ_{max}), oscillator strength (f) and transition obtained using method TD-DFT/B3YLP/6-311G

Molecules	E_{gap} (eV)	λ_{abs} (nm)	E_{ex} (eV)	f	Transition	Transition (%)
Diln 1	3.007	467.02	2.6548	1.2875	HOMO → LUMO	97.77
Diln 2	2.885	488.18	2.5397	1.2359	HOMO → LUMO	98.50
Diln 3	3.028	468.65	2.6456	1.0640	HOMO → LUMO	98.49
Diln 4	2.664	522.01	2.3751	1.3114	HOMO → LUMO	98.04
Diln 5	2.853	492.77	2.5161	1.2731	HOMO → LUMO	97.94
Diln 6	2.663	463.67	2.6751	1.2350	HOMO → LUMO + 1	96.81

5. CONCLUSION

In this research study, the DFT method with function B3LYP/6-311G has been used to evaluate the six proposed molecules' geometries, optoelectronic properties and reorganization energies. For improving the BHJ solar cell performance, six different π-conjugated molecules have been introduced and modified. Photovoltaic properties and absorption spectra of these compounds have been studied, discussed using the TD-DFT method with the identical functional and basis set (B3YLP/6-311G).

Using the DFT/B3LYP/6-311G method, the band gaps of molecules Diln 2 to Diln 6 are predicted to be lower than Diln 1 due to electron-releasing and electron-accepting groups substitution as the length of the conjugation is increased, which by supposed lower the band gap energies. The chemical potential of all the investigated diindole-based molecules being greater than that of PCBM predicts that the electrons can flow smoothly from studied molecules to PCBM. Moreover, the LUMO energies of all studied molecules and PCBM are all higher than the LUMO energy of ITO, which indicates that electrons are allowed to flow smoothly and thus

generates a current. It is observed that the calculated reorganization energies were found to be lowest for Diln 4 and highest for Diln 6. Hence, electron transport will be more rapid for Diln 4 compared to other investigated diindole-based molecules.

All studied compounds' absorption maximum wavelengths are found within the visible light region as calculated using TD-DFT/6-311G method with different functionals, *viz.*, B3LYP, CAM-B3LYP and WB97XD. Electronic transitions for all the studied molecules are also π-π*. Comparing all the methods, it is observed that the λ_{abs} of Diln 4 was found to be the highest using the TD-DFT/B3YLP/6-311G method. E_{gap} values of all the diindole-based molecules were found to be higher in the case of the TD-DFT/WB97XD/6-311G method, while the same values were found to be lower in the case of the TD-DFT/B3YLP/6-311G method. According to the data collected, the maximum wavelength increases as the energy band gap decreases. Thus, all the six studied molecules are suitable for electron donors in BHJ solar cells; meanwhile, PCBM behaves as the electron acceptor.

ACKNOWLEDGEMENTS

This work is supported by International Association for the Exchange of Students for Technical Experience (IAESTE) UK, International Association for the Exchange of Students for Technical Experience (IAESTE) India and Sikkim Manipal Institute of Technology (Ref. No.: IN-2020-50604-SU).

DECLARATIONS

Funding: Not Applicable

Conflicts of interest/Competing Interests: The authors declare that they have no known competing financial interests or personal relationships that could have appeared to influence the work reported in this paper.

Availability of Data and Material: Not Applicable

Code availability: Not Applicable

Authors' Contributions: E. T. L. Fei performed all computational studies and analyzed the data. J. Biswas involved in the conceptualization, design and manuscript drafting. B. Datta involved in the conceptualization, drafting and reviewing of the manuscript. D. Kumar helped analyze the data.

REFERENCE

1. Energy Matters (2020) Renewable Energy and Alternate Energy Sources. https://www.energymatters.com.au/components/renewable-energy. Accessed 14 July 2020.
2. Scharber MC, Sariciftci NS (2013) Prog Polym Sci 38:1929−1940.
3. (a) Hoppe H, Sariciftci NS (2004) J Mater Res 19:1924-1945; (b) Chen L-M, Hong Z, Li G, Yang Y (2009) Adv Mater 21:1434-1449; (c) Brabec CJ, Gowrisanker S, Halls JJM, Laird D, Jia S, Williams SP (2010) Adv Mater 22:3839-3856; (d) Dou L, You J, Yang J, Chen CC, He Y, Murase S, Moriarty T, Emery K, Li G, Yang Y (2012) Nat Photonics 6:180-185; (e) Oku T, Takeda A, Nagata A, Kidowaki H, Kumada K, Fujimoto K, Suzuki A, Akiyama T, Yamasaki Y, Ōsawa E (2013) Mater Technol 28:21-39; (f) Chen C-C, Chang W-H, Yoshimura K, Ohya K, You J, Gao J, Hong Z, Yang Y (2014) Adv Mater 26:5670-5677; (g) Chen J-D, Cui C, Li Y-Q, Zhou L, Ou Q-D, Li C, Li Y, Tang J-X (2015) Adv Mater 27:1035-1041; (h) Zheng Z, Zhang S, Zhang J, Qin Y, Li W, Yu R, Wei Z, Hou J (2016) Adv Mater 28:5133-5138.

4. Mayer AC, Scully SR, Hardin BE, Rowell MW, McGehee MD (2007) Mater Today 10:28–33.
5. Rafique S, Mah AS, Sulaiman K, Iwamoto M (2018) Renew Sustain Energy Rev 84:43–53.
6. Arbouch I, Karzazi Y, Hammouti B (2014) Phys Chem News 72:73-84.
7. Siddiki MK, Li J, Galipeau D, Qiao Q (2010) Energy Environ Sci 3:867–883.
8. Suraru S-L, Burschka C, Würthner F (2014) J Org Chem 79:128-139.
9. Wen Y, Xu J (2017) J Polym Sci A Polym Chem 55:1121-1150.
10. Gross EKU, Maitra NT (2012) In: Marques MAL, Maitra NT, Nogueira FMS, Gross EKU, Rubio A (Eds.) Fundamentals of Time-Dependent Density Functional Theory, Springer 53−99.
11. Frisch MJ, Trucks GW, Schlegel HB, Scuseria GE, Robb MA, Cheeseman JR, Montgomery JA Jr, Vreven T, Kudin KN, Burant JC, Millam JM, Iyengar SS, Tomasi J, Barone V, Mennucci B, Cossi M, Scalmani G, Rega N, Petersson GA, Nakatsuji H, Hada M, Ehara M, Toyota K, Ukuda R, Hasegawa J, Ishida M, Nakajima T, Honda Y, Kitao O, Nakai H, Klene M, Li X, Knox JE, Hratchian HP, Cross JB, Adamo C, Jaramillo J, Gomperts R, Stratmann RE, Yazyev O, Austin AJ, Cammi R, Pomelli C, Ochterski JW, Ayala PY, Morokuma K, Voth GA, Salvador P, Dannenberg JJ, Zakrzewski VG, Dapprich S, Daniels AD, Strain MC, Farkas O, Malick DK, Rabuck AD, Raghavachari K, Foresman JB, Ortiz JV, Cui Q, Baboul AG, Clifford S, Cioslowski J, Stefanov BB, Liu G, Liashenko A, Piskorz P, Komaromi I, Martin RL, Fox DJ, Keith T, Al-Laham MA, Peng CY, Anayakkara A, Challacombe M, Gill PMW, Johnson B, Chen W, Wong MW, Gonzalez C, Pople JA (2009) Gaussian 09, Revision A02. Gaussian Inc, Wallingford CT.
12. Becke AD (1993) J Chem Phys 98:5648–5652.
13. Lee C, Yang W, Parr RG (1988) Phys Rev B 37:785–789.
14. Raftani M, Abram T, Bennani N, Bouachrine M (2020) Results Chem 2:100040–100051.
15. Dias FB, Bourdakos KN, Jankus V, Moss KC, Kamtekar KT, Bhalla V, Santos J, Bryce MR, Monkman AP (2013) Adv Mater 25:3707–3714.
16. Aziz EA, Amine A, Bouzzine SM, Lachgar M, Hamidi M, Elhamzi A, Bouachrine M (2017) J Mater Environ Sci 8:3897–3905.
17. Verhoeven JW, Dirkx IP, de Boer, ThJ (1972) J Mol Spectrosc 42:149-160.

18. Raftani M, Abram T, Saidi W, Bejjit L, Bennani MN, Bouachrine M (2018) RHAZES: Green Appl Chem 2:92–102.
19. Zade SS, Zamoshchik N, Bendikov M (2011) Acc Chem Res 44:14–24.
20. Shao S, Shi J, Murtaza I, Xu P, He Y, Ghosh S, Zhu X, Perepichka IF, Meng H (2017) Polym Chem 8:769–784.
21. Bourass M, Benjelloun AT, Benzakour M, Mcharfi M, Hamidi M, Bouzzine SM, Bouachrine M (2016) Chem Cent J 10:67–77.
22. Amine M, Hamidi M, Bouzzine SM, Amine A, Bouachrine M (2012) Adv Mat Lett 3:15–20.
23. Abram T, Hsaine Z, Bejjit L, Hamidi M, Bouachrine M (2014) Inter J Adv Res Comput Sci Softw Eng 4:742–750.
24. Chattaraj PK, Maiti B (2003) J Am Chem Soc 125:2705–2710.
25. Pearson RG (1986) Proc Natl Acad Sci USA 83:8440–8441.
26. Murray JS, Sen K (1996) Molecular Electrostatic Potentials: Concepts and Applications. 1st ed., Elsevier Science.
27. Bouzayen N, Mbarek M, Alimi K (2015) Mor J Chem 3:28–39.
28. Scrocco E, Tomasi J (1978) Adv Quantum Chem 11:115–193.
29. Shakila G, Saleem H, Sundaraganesan N (2017) World Sci News 61:150–185.
30. Ohkita H, Cook S, Astuti Y, Duffy W, Tierney S, Zhang W, Heeney M, McCulloch I, Nelson J, Bradley DDC, Durrant JR (2008) J Am Chem Soc 130:3030–3042.
31. Troshin PA, Lyubovskaya RN, Razumov VF (2008) Nanotechnol Russ 3:242–271.
32. Assyry AE, Jdaa R, Benali B, Addou M, Zarrouk A (2015) J Mater Environ Sci 6:2612–2623.
33. Youssef AA, Bouzzine SM, Fahim ZME, Sidir I, Hamidi M, Bouachrine M (2019) Physica B Condens Matter 560:111–125.
34. Zhang Z-L, Zhou L-Y, Ren A-M, Liu Y-F, Feng J-K, Sun C-C (2013) Dyes Pigm 96:349–363.
35. Chandrasekaran J, Nithyaprakash D, Ajjan KB, Maruthamuthu S, Manoharan D, Kumar S (2011) Renew Sustain Energy Rev 15:1228–1238.
36. Frohne H, Shaheen SE, Brabec CJ, Müller DC, Sariciftci NS, Meerholz K (2002) ChemPhysChem 3:795–799.

37. Wu Z, Fan B, Xue F, Adachi C, Ouyang J (2010) Sol Energy Mater Sol Cells 94:2230–2237.
38. O'Boyle NM, Tenderholt AL, Langner KM (2008) J Comput Chem 29:839–845.
39. Jin RF, Wang K (2015) Int J Mol Sci 16:20326–20343.
40. Kose ME, Mitchell WJ, Kopidakis N, Chang CH, Shaheen SE, Kim K, Rumbles G (2007) J Am Chem Soc 129:14257–14270.
41. Chrostowska A, Xu S, Mazière A, Boknevitz K, Li B, Abbey ER, Dargelos A, Graciaa A, Liu S-Y (2014) J Am Chem Soc 136:11813-11820.

Figures

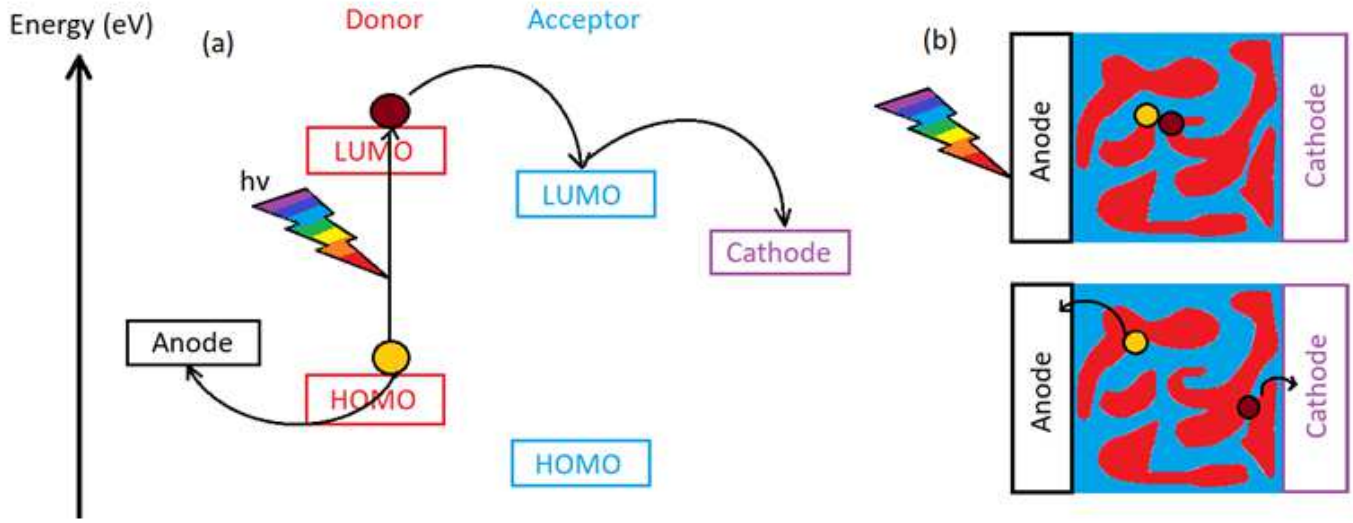

Figure 1

(a) Schematic diagram on photocurrent generation in the active layer of BHJ solar cell. (b) Simpler illumination on the separation of excitons and the transfer of free charge carriers to respective electrodes.

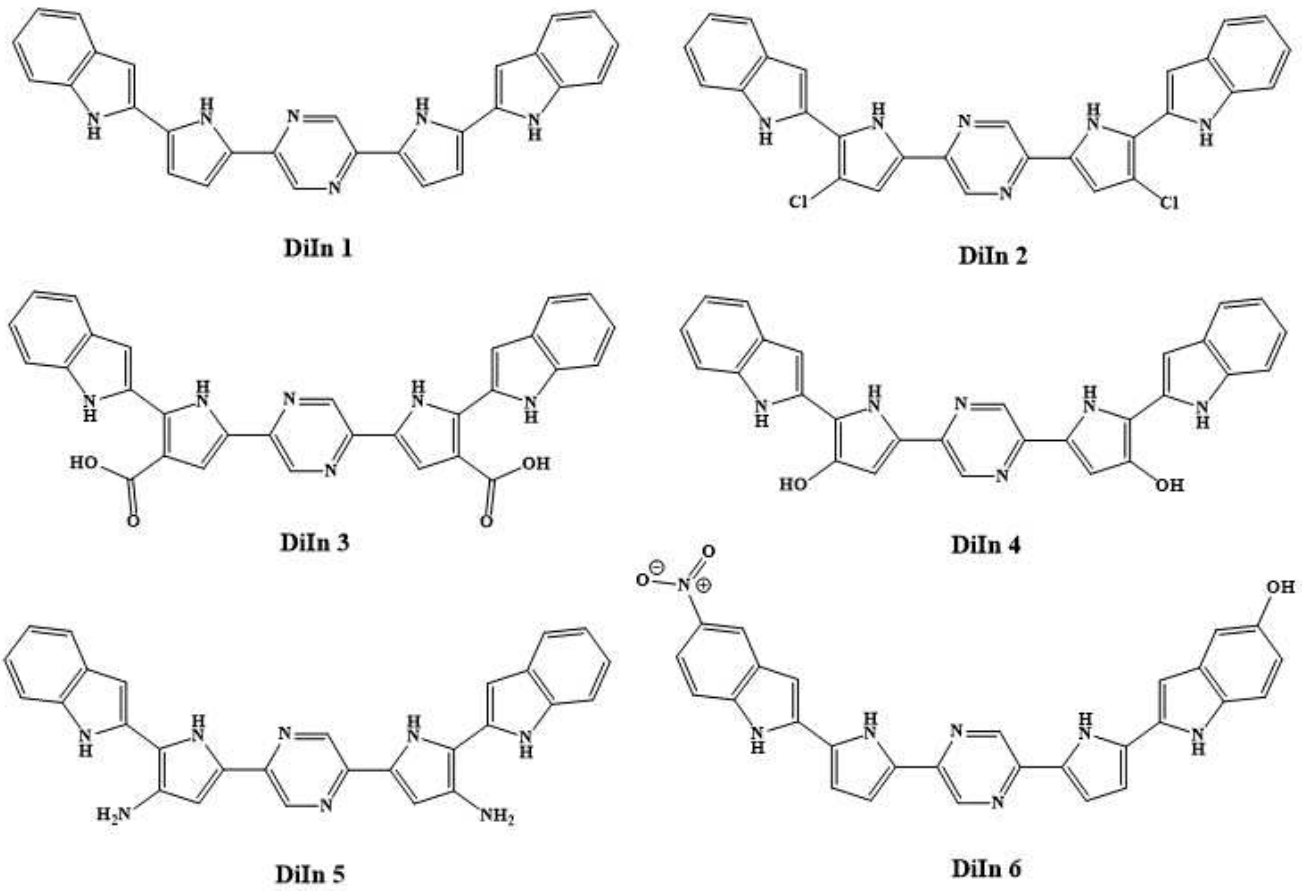

Figure 2

Chemical structures of introduced molecules.

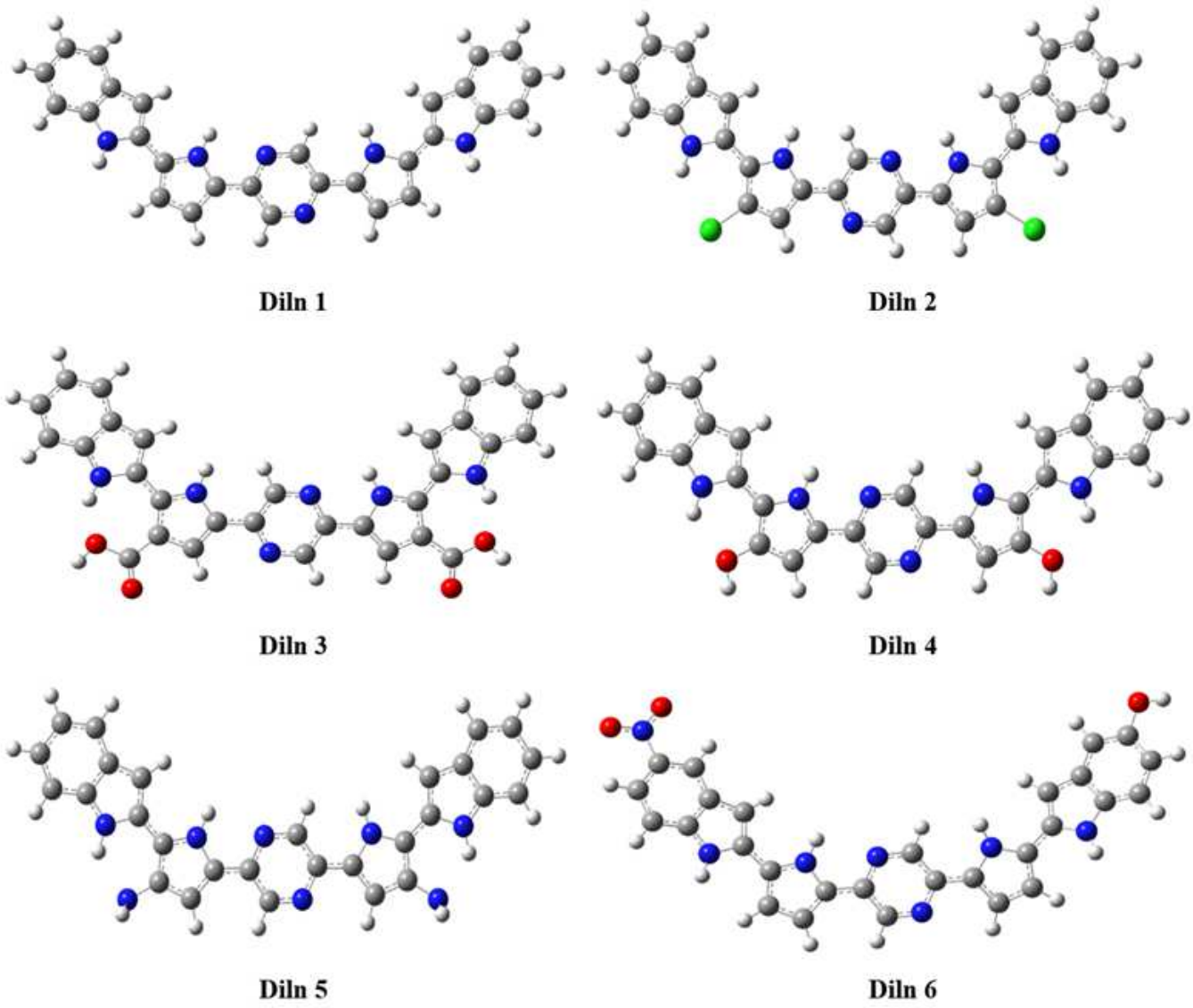

Figure 3

Energy-minimized structures of all the investigated molecules using DFT/B3YLP/6-311G.

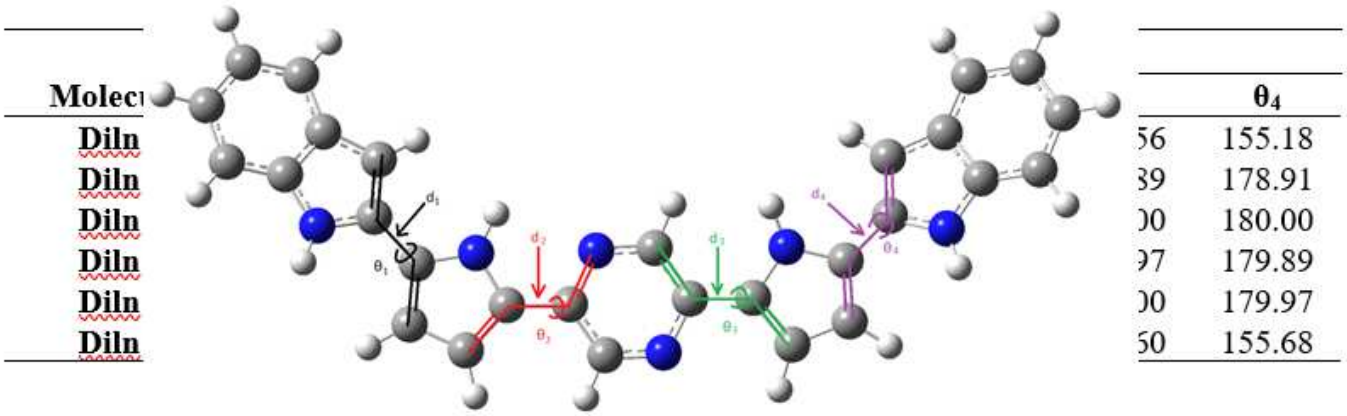

Molecu	θ_4
Diln	56 155.18
Diln	39 178.91
Diln	00 180.00
Diln	97 179.89
Diln	00 179.97
Diln	50 155.68

Figure 4

Illustration of selected geometries parameters.

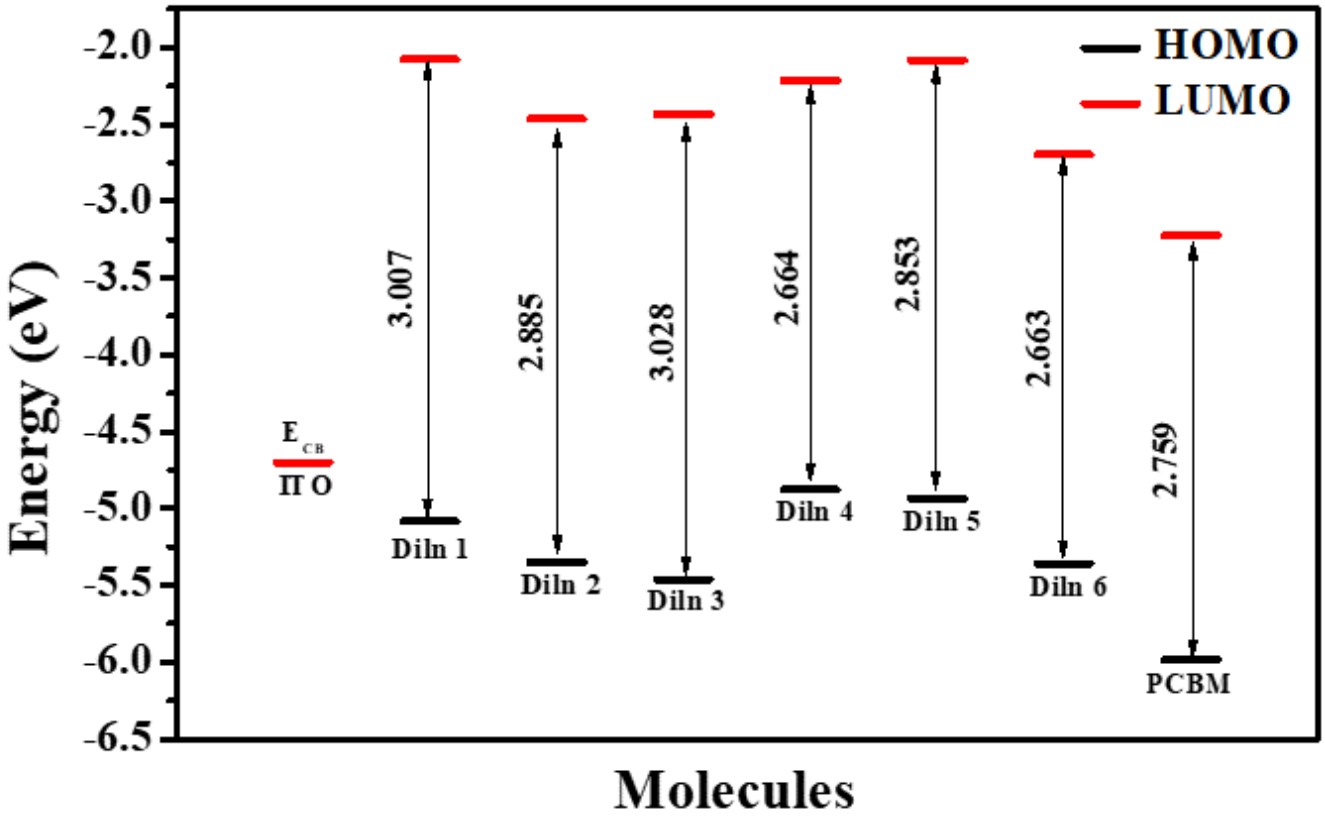

Figure 5

Calculated HOMO and LUMO energy levels (in eV) of all the studied diindole-based molecules, PCBM and ITO.

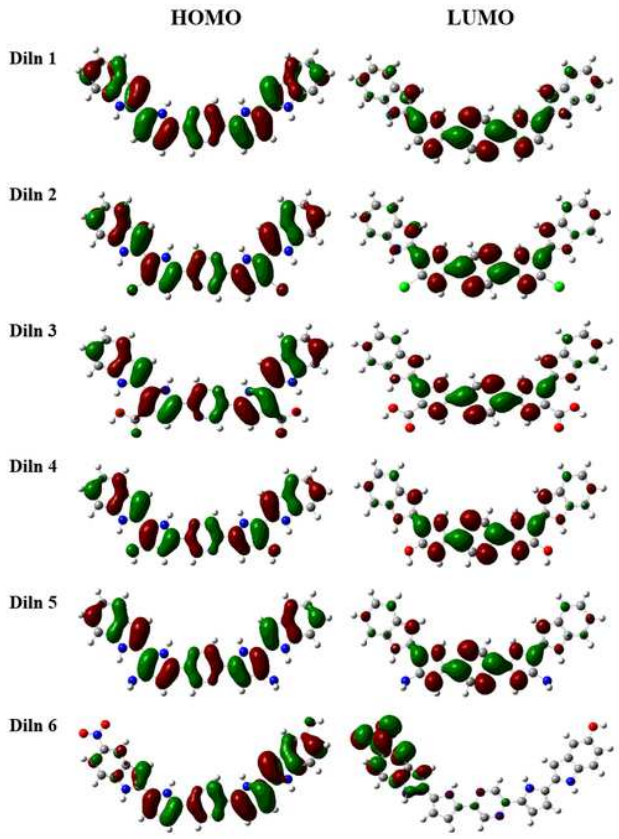

Figure 6

The contour plots of HOMO and LUMO orbitals of studied diindole molecules.

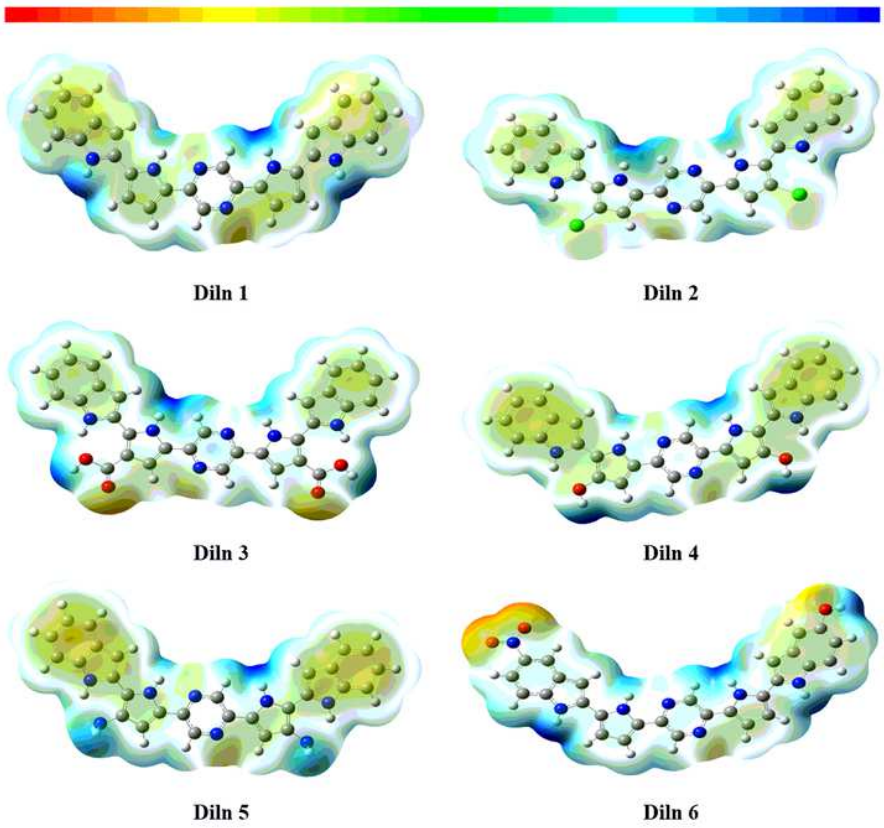

Figure 7

Molecular electrostatic potential of studied molecules using DFT/B3YLP/6-311G.

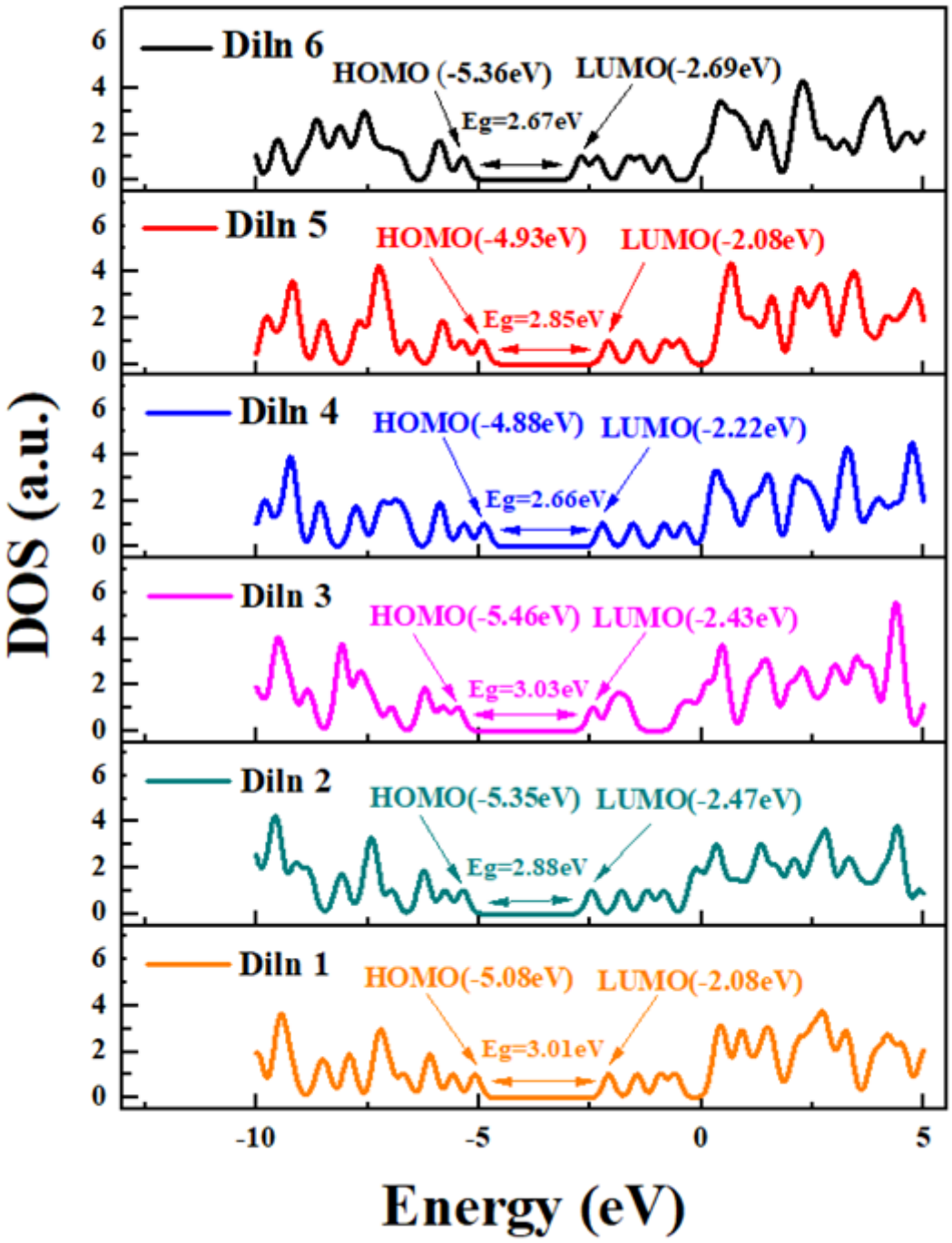

Figure 8

DOS (density of states) studies carried out using GaussSum software.

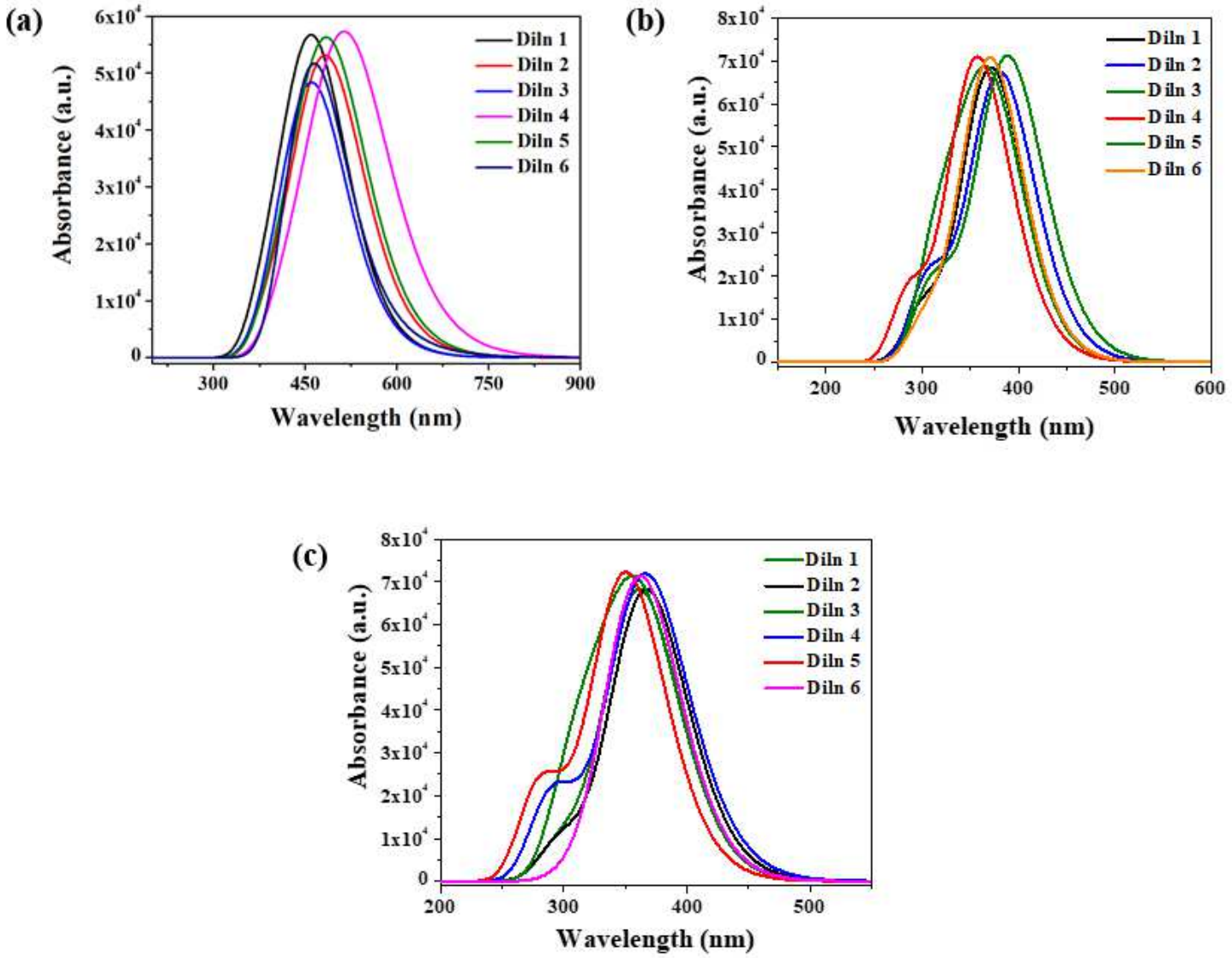

Figure 9

Theoretically obtained UV-Vis spectra of all the investigated diindole-based molecules using (a) TD-DFT/B3YLP/6-311G, (b) TD-DFT/CAM-B3YLP/6-311G and (c) TD-DFT/WB97XD/6-311G.

Supplementary Files

This is a list of supplementary files associated with this preprint. Click to download.

- GraphicalAbstract.jpg
- SupplementaryData.doc